A Model To Predict Long-Term Performance of Vapor-Phase Bioreactors: A Cellular Automaton Approach

ARTICLE *in* ENVIRONMENTAL SCIENCE AND TECHNOLOGY · JULY 2002

Impact Factor: 5.33 · DOI: 10.1021/es0156183 · Source: PubMed

2 AUTHORS, INCLUDING:

Kerry A Kinney
University of Texas at Austin
104 PUBLICATIONS **1,184** CITATIONS

Environ. Sci. Technol. **2002**, *36,* 2498−2507

A Model To Predict Long-Term Performance of Vapor-Phase Bioreactors: A Cellular Automaton Approach

JIHYEON SONG AND KERRY A. KINNEY*

Environmental and Water Resources Engineering, Department of Civil Engineering, ECJ 8.6, University of Texas at Austin, Austin, Texas 78712

A novel numerical model was constructed to predict performance of vapor-phase bioreactors (VPBs) operated over extended periods. This model incorporates two unique features to simulate changes in pollutant removal efficiency and biomass accumulation: (1) total biomass is divided into two microbial components, active and inactive biomass, and (2) biomass growth and biofilm thickness changes are simulated by means of a cellular automaton (CA) approach. The CA approach, a differential-discrete algorithm, numerically allows the excess quantity of biomass in each numerical element to move toward the biofilm surface as biomass accumulates. One set of experimental bioreactor data was used to estimate unknown model parameters. A 90-day simulation using the estimated parameters agreed with pollutant removal and biomass accumulation profiles determined experimentally. Four additional model simulations using the same estimated model parameters were generally consistent with experimental data collected from a series of toluene-degrading VPBs operated over a range of conditions. Model predictions imply that the decline in bioreactor performance observed over extended operation was caused by a decline in the active biomass fraction and a decrease in the biofilm specific surface area. This CA model provides insight into biomass accumulation during complex bioreactor operation and improves our capability to predict long-term VPB performance.

Introduction

Since vapor-phase bioreactors (VPBs) have emerged as a viable treatment technology for volatile organic compounds from various sources, many numerical models have been developed to predict VPB performance (*1*−*9*). First- and zero-order kinetic expressions have been widely used for the biodegradation process (*1*−*3*), while Monod type models with inhibition effects and dual substrates have been explored by several investigators (*4*−*6*). Models that take into account potential limiting factors have also been proposed, including nitrogen limitations (*7*) as well as pH changes resulting from CO_2 accumulation and acid formation during the biodegradation processes (*8*, *9*).

Efforts to model VPB processes have focused mainly on pseudo-steady-state conditions or short-term transient responses. A common pseudo-steady-state assumption is that the density and composition of the biofilm are homogeneous along the bioreactor column and constant with time (*1*−*8*). For these pseudo-steady-state assumptions to be true, most conventional models have been restricted to simulating short periods of operation (e.g., less than a few days) when bioreactor performance is steady. These models have difficulties predicting long-term bioreactor performance accurately, since non-steady-state conditions are encountered frequently in VPB operation.

Excess biomass accumulation and declines in pollutant-degrading activity are commonly observed in VPBs operated for long periods at high organic loading rates (*10*−*13*). In addition, biofilm systems in mixed-culture VPBs are heterogeneous, containing active microbial components that actively degrade pollutants and inactive microbial components that consist of secondary microbial populations, dead cells and exopolymeric substances. Changes in the relative quantities of these microbial components can lead to a decline in overall bioreactor performance (*12*, *13*). Models that incorporate this complexity are required to improve predictions of VPB performance over long-term operation.

Several numerical models have recently been proposed to estimate temporal and spatial changes in biofilm thickness and population dynamics using differential equations to describe the relevant physical and biochemical processes (*9*, *14*−*16*). These models have adapted a biomass convective flux concept, in which biofilm thickness varies with time at a given biofilm expansion rate. Although these models include changes in biofilm thickness and specific surface area as a function of biomass growth, biomass density and activity are assumed to be constant. An alternative approach proposed by Okkerse et al. (*9*) incorporates an active biomass fraction (f_{act}) and an inert biomass fraction (f_{inert}) into the VPB model to distinguish microbial components in the biofilm phase.

A new mathematical approach based on a differential-discrete cellular automaton (CA) algorithm has recently been developed to predict biomass growth and spatial heterogeneities in a biofilm (*17*−*20*). The CA algorithm numerically constructs a network of discrete grids in the biofilm domain, and biofilm growth is simulated by relocating excess microbial component to the next available grid. As the quantity of each microbial component changes, biomass density is also altered in each discrete grid. The CA approach is computationally and conceptually advantageous since it is relatively easy to formulate numerical solutions, and it better describes the spatial heterogeneity of biofilms. Pizarro et al. (*18*) constructed a fully quantitative CA model that described both substrate and biomass as discrete particles in a numerical domain. In another approach, Picioreanu et al. (*19*, *20*) developed a hybrid CA model that used differential equations for substrate diffusion but employed the CA algorithm for biomass growth.

In this study, a novel mathematical model that incorporates biofilm growth and two microbial (active and inactive) components in the biofilm was constructed. The main objectives of this study were to demonstrate the utility of a hybrid type CA model for complex VPB systems and to provide quantitative predictions of bioreactor performance and biomass accumulation over long-term periods. Data collected from five bioreactors, operated in either unidirectional (UD) or directionally switching (DS) mode and subjected to a range of inlet toluene concentrations (Table 1), were used to calibrate and validate the model. These operating conditions were selected for modeling purposes since the substantial changes in biomass and pollutant degradation observed in

* Corresponding author phone: (512)232-2579; fax: (512)471-1720; e-mail: kakinney@mail.utexas.edu.

TABLE 1. Bioreactor Operating Conditions[a]

expt	bioreactor	days of operation	directionally-switching[b] operation	inlet toluene concn (ppm_v)	inlet toluene loading (g/m^3-h)
1	DS-3-day	78	3 day SF[c]	200	45.8
2	DS-7-day	68	7 day SF	200	45.8
3	UD	96	No	200	45.8
4	DS-400	45	3 day SF	200 (days 0−23), 400 (days 24−45)	45.8 91.1
5	DS-600	47	3 day SF	200 (days 0−23), 600 (days 24−47)	45.8 136.7

[a] A packed bed volume of 19.8 L, an air flowrate of 19.8 L/min, and an empty bed residence time of 1 min were used in all VPB experiments. [b] Directionally switching operation in which the direction of the air flow was periodically reversed throughout the bioreactor column, i.e., every 3 or 7 days. [c] Switching frequency.

each experiment (*12*, *21*) allowed comparison with model simulations. In the UD bioreactor, a skewed biomass distribution developed quickly in the column along with a relatively rapid loss in pollutant degradation capacity near the bioreactor inlet. In the DS bioreactors, where the gas flow direction was periodically reversed between the top and bottom of the bioreactor column, a more uniform distribution of active biomass was observed. However, even in DS operation, substantial changes in toluene removal and biomass accumulation still occurred, particularly when the inlet pollutant loading was increased.

Model Development

General Assumptions. This model describes a VPB in which a mixed-culture biofilm is growing on the surface of a solid, pelletized packing material. In the bioreactor described herein, no free liquid is recirculated through the packing materials, but water and nutrients are continuously supplied using a nutrient-laden aerosol to minimize the effect of nutrient limitation on biofilm growth. As shown in the conceptual diagram in Figure 1(a), overall VPB processes take place in two phases linked by one interface; the gas phase, the biofilm phase containing two different biomass components, and a thin interfacial layer between the gas/biofilm phases. This model is also constructed to adapt to a change in gas flow direction; thus, it can be used to predict bioreactor operation in either a unidirectional (UD) feed mode or in a directionally switching (DS) feed mode. The general assumptions made in deriving this model are as follows: (1) The biofilm is treated as a planar surface. (2) One substrate (toluene) is rate-limiting. (3) Toluene at the gas/biofilm interface is always in equilibrium as described by Henry's law. There is a concentration gradient (interfacial resistance) in the interfacial layer (Figure 1). (4) Diffusion/reaction inside the biofilm occurs in one direction only (1D model). (5) Toluene transport in the biofilm is by diffusion only, and the diffusivity of toluene is assumed to be constant throughout the biofilm. (6) The biofilm consists of two different biomass components: active biomass (X_{act}) and inactive biomass (X_{inact}) (i.e., $X_{total} = X_{act} + X_{inact}$). The concentration of each biomass component varies inside the biofilm along the column length and with time. (7) Only X_{act} is capable of degrading toluene. X_{act} increases with microbial growth resulting from toluene biodegradation but decreases with microbial decay resulting from endogenous respiration and irreversible losses such as inactivation of X_{act}. (8) Microbial growth is described by Monod type kinetics, and kinetic coefficients are assumed to remain constant. (9) Microbial decay is assumed to be proportional to the active biomass concentration. A fraction of active biomass decays and is converted into inactive biomass (X_{inact}), e.g., dead cells

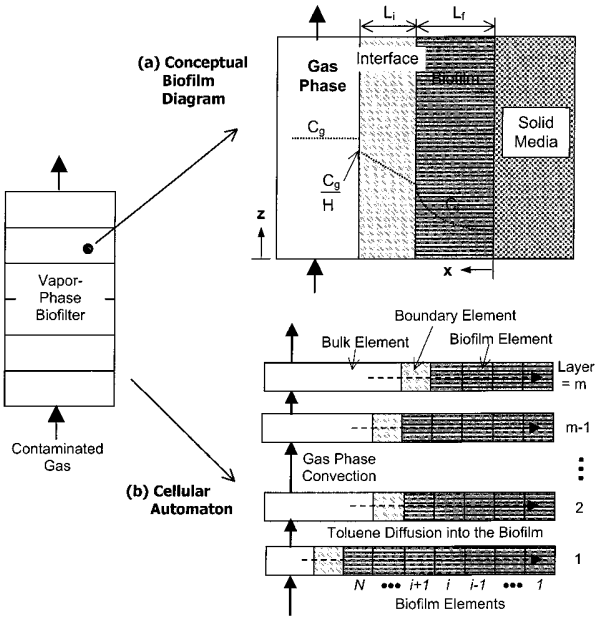

FIGURE 1. (a) Conceptual diagram of the gas and biofilm phases in the VPB model and (b) description of the numerical domain used for the cellular automaton approach. The dotted line in (a) represents the pollutant concentration, and the dotted arrows in (b) represent toluene diffusion into the biofilm elements. For numerical purposes, the bioreactor column is conceptually divided into layers (12 in these simulations) with identical dimensions, and each is connected by gas-phase advection.

and extracellular polymeric substances. (10) The gas stream passes through this packed bed bioreactor in a plug flow manner; therefore, the diffusive mass transfer of toluene in the gas phase is negligible.

Mass Balance and Model Equations. Based on the above assumptions, model equations and boundary conditions are constructed as follows:

1. Mass Balance in the Gas Phase. In the plug-flow reactor, the change in toluene concentration in the gas phase is a function of the advective flux of toluene along the column and the diffusive flux of toluene from the gas phase to the biofilm phase due to the concentration difference across the interfacial layer (see Figure 1(a))

$$\frac{\partial C_g}{\partial t} = -\frac{v}{\epsilon_f}\frac{\partial C_g}{\partial z} - Ja_f, \quad \text{and}$$

$$J = k_L\left(\frac{C_g}{H} - C_{l,x=Lf}\right) \quad @z = 0,\ C_g = C_{g,in} \quad (1)$$

where C_g is the toluene concentration in the gas phase (mg/L_{gas}), $C_{g,in}$ is the inlet toluene concentration (mg/L_{gas}), v is the superficial gas velocity (m/h), ϵ_f is the porosity of the packed bed (m^3 void space/m^3 reactor volume), a_f is the specific biofilm surface area (m^2/m^3), J is the diffusive flux of toluene from the gas phase to the biofilm (mg/m^2-h), $C_{l,x=Lf}$ is the toluene concentration at the biofilm interface (mg/L_{liquid}), L_f is the total biofilm thickness (m), k_L is the mass transfer coefficient (m/h), and H is Henry's law constant (mg/L_{gas}/mg/L_{liquid}).

2. Mass Balance in the Biofilm Phase. Toluene diffusion and biodegradation take place in the biofilm phase, as described by the following mass balance equation using Monod kinetics. As indicated in the general assumptions, only active biomass (X_{act}) is responsible for toluene biodegradation

$$\frac{\partial C_l}{\partial t} = D_f \frac{\partial^2 C_l}{\partial x^2} - \frac{\mu_m C_l}{K_s + C_l} \frac{X_{act}}{Y_{act}} \quad @x = 0, \frac{dC_l}{dx} = 0, \quad \text{and} \quad @x = L_f, C_l = C_{l,x=Lf} \quad (2)$$

where C_l is the toluene concentration in the liquid phase (mg/L_{liquid}), D_f is the effective diffusion coefficient of toluene (m^2/h), μ_m is the maximum growth rate of X_{act} (1/h), K_s is the Monod half saturation constant (mg/L), X_{act} is the microbial density of the active microbial component (mg COD/L), and Y_{act} is the yield coefficient of X_{act} ($mg\ COD_{biomass}/mg_{toluene}$).

3. Biomass Growth in the Biofilm Phase. The net accumulation of X_{act} is the difference between microbial biomass growth and biomass decay. Biomass decay is a complicated microbial process that can include endogenous respiration, cell death, and extracellular polymer secretion in the biofilm phase. In this model, biomass decay is assumed to be proportional to X_{act}, and a fraction of X_{act} is converted into inactive biomass (X_{inact}) such as cell debris and extracellular polymeric substances. Since biofilm detachment is negligible in a bioreactor system without a recirculating liquid stream and inactive biomass is assumed to be high molecular weight polymers or dead cells, a loss term is not included in the equation for X_{inact}.

$$\frac{\partial X_{act}}{\partial t} = \frac{\mu_m C_l}{K_s + C_l} X_{act} - k_d X_{act} \quad @t = 0, X_{act} = X_{act,o} \quad (3)$$

$$\frac{\partial X_{inact}}{\partial t} = \beta k_d X_{act} \quad @t = 0, X_{inact} = X_{inact,o} \quad (4)$$

where k_d is the biomass decay rate (1/h), X_{inact} is the microbial density of the inactive microbial component (mg COD/L), and β is the formation coefficient for X_{inact} (−).

4. Changes in Biofilm Thickness (Cellular Automaton Approach). Changes in biomass density calculated using the two partial differential equations above (eqs 3 and 4) are used to determine the increase in biofilm thickness by means of a cellular automaton algorithm (i.e., the discrete-differential approach). In the algorithm, the numerical domain is divided into discrete grids that consist of biofilm, boundary, and bulk elements (*17*). A conceptual diagram of this scheme is provided in Figure 1(b). Only biofilm elements contain microbial components (X_{act} and X_{inact}), and each biofilm element is linked through diffusive mass transfer. The boundary elements at the gas/biofilm interface mediate the mass transfer between the two phases, but they do not contain microbial components. The bulk elements are filled with toluene at a constant gas-phase concentration. As the overall biomass quantity increases, each interfacial grid in the biofilm phase moves to the next available grid according to the cellular automaton algorithm (*19*, *20*).

The sum of each microbial component in each biofilm element can vary from zero to a maximum hypothetical density (X_{set}). This allows the biomass density and composition within the biofilm to change with time. When the sum of the two microbial components ($X^i_{total} = X^i_{act} + X^i_{inact}$) in the ith biofilm element exceeds the maximum density (X_{set}), the excess microbial quantity ($X^i_{excess} = X^i_{total} - X_{set}$) is moved to the next, i+1th biofilm element. The excess biomass quantity of each microbial component is transferred from the ith element at a ratio proportional to its fraction in the ith element. For example, the concentration of the active microbial component in the ith biofilm element after the excess quantity has been transferred out of the element is

$$X^i_{act}(t^*) = X^i_{act}(t) - X^i_{excess} \frac{X^i_{act}(t)}{X^i_{total}(t)}, \text{ if } X^i_{total} > X_{set} \quad (5)$$

where $X^i_{act}(t)$ is the concentration of the active microbial component in the ith biofilm element at time t (mg/m^3), and $X^i_{act}(t^*)$ is the concentration of the active microbial component in the ith biofilm element after the excess biomass quantity has been transferred from the element (mg/m^3). The concentration of each microbial component in the i+1th biofilm element is recalculated by adding each microbial quantity transferred from the ith element to those previously present in the element. If the total microbial density in a biofilm element does not exceed the maximum limit, no reallocation occurs. These redistributions of microbial components continue from the biofilm element adjacent to the packing material (i.e., $i = 1$) to the outermost biofilm element ($i = N$). In this 1D model, biomass movement is always toward the biofilm surface (i.e., expansion only), and biofilm detachment or shrinkage is not considered. If the total microbial concentration exceeds the maximum density in the outermost biofilm element, a new biofilm element is created between the outermost biofilm and the boundary elements. In this manner, biofilm expansion increases the number of biofilm elements, while the location of the boundary element is sequentially moved outward in the numerical domain. The rearranged biomass distribution within the biofilm is used to predict mass transfer and biodegradation of toluene for the next time step. The new biofilm thickness (L_f) is calculated using the following equation

$$L_f = N \times W \quad (6)$$

where N is the number of the biofilm elements at each time step (see Figure 1(b)), and W is the width of each biofilm element (m). In this study, each biofilm element is assumed to be a cubicle with a width of 2.5×10^{-6} m, a value within the range used successfully by other researchers (*18*−*20*). The size of the biofilm element is considered to be a numerical construct, and no attempt is made to correlate this value with real biofilm clusters. Additional research would be required to directly relate this value to heterogeneous biofilm systems since biofilm clusters are highly variable and dependent on environmental conditions.

5. Changes in Specific Surface Area (a_f) and Porosity (ϵ_f). An increase in biofilm thickness changes the specific surface area of the biofilm (a_f) and the corresponding packing bed porosity (ϵ_f). Alonso et al. (*14*, *15*) formulated equations for specific surface area and packing bed porosity, based on a packing spheres model where the biofilm expands into the void space left between the packing materials. The changes in a_f and ϵ_f can be expressed as a function of biofilm thickness (L_f)

$$a_f = \frac{3(1-\epsilon_0)}{2R\phi}\left(1 + \frac{L_f}{R}\right)\left((2-n)\frac{L_f}{R} + 2\right) \quad (7)$$

$$\epsilon_f = 1 - (1-\epsilon_0)\left[\left(1 + \frac{L_f}{R}\right)^3 - \frac{n}{4}\left(\frac{L_f}{R}\right)^2\left(3 + 2\frac{L_f}{R}\right)\right] \quad (8)$$

where ϵ_0 is the clean bed porosity, ϕ is the sphericity factor of pelletized packing materials, n is the coordinate number of the characteristic packing spheres in contact with a given sphere, and R is the characteristic packing sphere radius (m). Since the packing material (porous silicate pellets, Celite R-635, Celite Co., CA) used in this study was also used in the study by Alonso et al. (*14*, *15*), the same model parameters developed in their model studies were adapted for this study; i.e., coordinate number ($n = 10$), clean bed porosity ($\epsilon_o = 0.34$), and sphericity factor of pelletized packing materials ($\phi = 0.857$).

Time Scale. Physical, chemical, and biological processes in a VPB take place on different time scales. Diffusion and

biodegradation processes have much shorter characteristic times than changes in biomass quantity (growth, injury, and decay). In general, substrate diffusion and reaction are at least 10 times faster than biomass growth (*20*). The mass balance equations for the gas and biofilm phases can, therefore, be considered to be at a quasi steady-state for a given biomass distribution. As a result, the partial differential equations (eqs 1 and 2) can be simplified to coupled ordinary equations as follows:

$$0 = -\frac{v}{\epsilon_f}\frac{\partial C_g}{\partial z} - k_L a_f\left(\frac{C_g}{H} - C_{l,x=Lf}\right) \quad (9)$$

$$0 = D_f\frac{\partial^2 C_l}{\partial x^2} - \frac{\mu_m C_l}{K_s + C_l}\frac{X_{act}}{Y_{act}} \quad (10)$$

This assumption can provide stability and convergence to the numerical solutions. Alonso et al. (*15*) showed that a solution using the quasi steady-state assumption did not significantly differ from the simulation results solved without this assumption. In the numerical algorithm of the model developed in this study, a quasi-steady-state profile of toluene concentration was calculated first assuming a fixed biomass distribution. Then, the new biomass quantity in the numerical domain was calculated according to the toluene profile. Trial simulations performed at time intervals of 6 and 12 min yielded almost identical results with less than a 5% difference in overall toluene removal predictions over a 50-day simulation. As a result, the 12-min (0.2 h) time interval was used in this study to save computational time.

Numerical Approach. If each computational segment is small enough, a packed bed reactor can be considered to be a series of well-mixed reactors. For modeling purposes, the bioreactor column is divided into a series of well-mixed layers for the gas phase, and each gas phase reactor is combined with a biofilm reactor through a diffusive link, as shown in Figure 1(b). In each bioreactor layer, the bulk gas phase concentration was determined by averaging the toluene concentrations of the gas entering and exiting the layer. In the simulations reported herein, the bioreactor was divided into 12 equal volume layers of gas and biofilm phases. Model simulations with 24 equal layers were also conducted for a 50-day period using the same model parameters. The two simulations resulted in only a 1% discrepancy in predicted overall toluene removal efficiency. Therefore, all simulations in this study were performed using 12 layers along the VPB column.

The mass balance for the biofilm phase (eq 10) and the gas-phase flux equation (eq 9) were converted to a paired set of equations using a finite difference scheme for a boundary value problem, and the equations were solved by the Gauss-Seidel iteration method (*22*). Multiple iterations were required when dealing with this nonlinear, moving boundary problem.

Parameter Estimation. A weighted least-squares error method was employed to estimate each model parameter in the coupled nonlinear equations (*23*). Since this model is constructed to simulate VPB performance with respect to toluene removal efficiency along the bioreactor column and biomass accumulation over time, normalized profiles of toluene and biomass along the VPB column length were used for parameter estimation. The equation below represents the objective function used in this study to minimize the sum of squared errors (SSE) between the actual experimental data and the simulated values for the set of estimated parameters

$$\text{minimize SSE}(p) = \sum_i \frac{1}{2}(f_{toluene,measured} - f_{toluene}(p))^2 + \sum_j \frac{1}{2}(f_{biomass,measured} - f_{biomass}(p))^2, \quad \text{and}$$
$$p = (p_1, p_2, \cdots, p_m) \quad (11)$$

where $f_{measured}$ is the experimentally measured value, f(p) is the simulated value using a set of estimated parameters, and $p = (p_1, p_2, ..., p_m)$ is the set of estimated parameters. Because toluene removal and biomass concentration were considered to be key operating parameters, both were weighted equally in the objective function.

Materials and Methods

Bioreactor Configuration and Operation. Results obtained from five lab-scale VPB experiments were used in this study. The bioreactors were configured identically and consisted of stainless steel columns with an inner diameter of 16.2 cm (see Figure SI-1, Supporting Information). Each column was packed with pelletized biological support media (Celite R-635, Celite Co., CA) to an overall bed height of 1.0 m. Toluene was used as a model volatile organic compound for all the bioreactor column studies. The air stream to the bioreactor was contaminated with toluene and saturated with a nutrient-laden aerosol to continuously supply nutrients and moisture to the column. Table 1 summarizes the operating conditions for each of the five experiments. Four bioreactors (DS-3-day, DS-7-day, DS-400, and DS-600 in Table 1) were operated in a directionally switching (DS) mode, such that the direction of the air stream through the bioreactor column was periodically reversed. In previous studies, DS operation has been shown to allow extended bioreactor operation by promoting a more even biomass distribution along the column (*12*, *21*). For comparison purposes, one bioreactor (UD in Table 1) was operated in a unidirectional manner with the contaminated air flow continuously supplied to the bottom of the column. Details regarding bioreactor configuration, operation, and inoculation as well as the chemical composition of the nutrient-laden aerosol used in this study have been described previously (*12*, *21*).

Analytical Methods. Previous column studies have demonstrated that overall removal efficiencies and concentration profiles along the bioreactor column can be used to monitor bioreactor performance (*12*, *21*). To measure toluene concentrations, gas samples were collected from gas sampling ports and analyzed immediately using a gas chromatograph (series 6890, Hewlett-Packard, CA) equipped with a flame ionization detector. The gas sampling ports were located at 0, 0.25, 0.5, 0.75, and 1 m along the bioreactor column (Figure SI-1, Supporting Information). Chemical oxygen demand (COD) was employed to determine biomass accumulation. Biofilm samples (biomass-covered pellets) were collected from packing media sampling ports located at 0.08, 0.33, 0.67, and 0.92 m along the column and analyzed using a COD vial (Hach, CO). A detailed description of the analytical procedures is reported elsewhere (*12*).

Results and Discussion

The model presented herein was developed to predict the changes in bioreactor performance as well as biomass accumulation and distribution that occur in VPBs with increasing operation time. Model parameters were estimated by fitting the model to experimental data collected from a toluene-degrading VPB (DS-3-day, Table 1). Using the same estimated model parameters, model predictions were validated and compared with actual experimental data collected from a series of toluene-degrading VPBs operated under a range of conditions (DS-7-day, UD, DS-400 and DS-600).

TABLE 2. Model Parameter Values Used in This Study and Sensitivity Indexes

	parameters	value	units	values used as starting points for fitting	ΔSSE[a]
estimated	μ_m (maximum growth rate)	0.05	1/h	0.028[b]	0.019
	K_s (half-saturation constant)	0.10	mg/L	0.29[b]	0.002
	Y_{act} (yield coefficient)	0.76	mgCOD/L	0.80[b]	0.027
	k_d (biomass decay rate)	0.016	1/h	0.018 (*14*)	0.058
	β (inactive biomass formation)	0.17	mg/mg	0.13 (*9*)	0.001
	X_{set} (maximum biomass density)	25.0	g/L	17.0 (*14*)	0.032
	k_L (mass transfer coefficient)	2.8	m/h	1.8 (*9*)	0.083
known	Z (total biofilter height)	1.0	m		
	V (total packed volume)	19.8	L		
	Q (gas-phase flowrate)	1188	L/h		
	H (Henry's law constant)	0.265 (*24*, *25*)	mg/L/mg/L		
	D_f (toluene diffusion coefficient)	3.5×10^{-6} (*24*, *25*)	m^2/h		
	R (packing sphere radius)	0.003 (*14*)			
	ϕ (sphericity of packing)	0.857 (*14*)			
	ϵ_0 (clean bed porocity)	0.340 (*14*)			
	n (number of characteristic spheres)	10 (*14*)			
initial conditions (estimated)	L_{f0} (initial biofilm thickness)	15.0	μm	15.0	0.003
	L_{f0} for UD simulation only	37.5	μm		0.023[c]
	X_{act0} (initial X_{act})	4.0	g/L	1.6	0.002
	X_{inact0} (initial X_{inact})	0.0	g/L	0.0	0.001[d]

[a] Differences between SSE_o (the SSE calculated using eq 11 with nominal parameter values) and SSE_j (the SSE when each parameter is increased by 10% while the others remain unchanged). [b] Experimentally determined in batch kinetic tests. [c] ΔSSE resulting from modifying the initial biofilm thickness estimate from 15.0 to 37.5 μm for UD simulation only. [d] Used X_{inact0} of 0.1 g/L to calculate SSE_j.

Model Parameter Estimation and Sensitivity. Parameter estimation was performed by optimizing the objective function (eq 11) using the toluene removal and biomass profiles determined in the DS-3-day column on day 75. Six parameters were obtained from the literature (*14*, *24*, *25*), while three initial conditions and seven unknown parameters were fit to the experimental data using the objective function. Parameter values reported in the literature for similar VPB models were used as starting points in the estimation process for four of the seven unknown parameters (Table 2). For example, Alonso et al. (*14*) employed a decay rate coefficient of 0.018 h^{-1}, and this value was used as the initial estimate for the biomass decay rate (k_d). The starting points for the other three unknown parameters, the microbial kinetic coefficients, were based on experimental results obtained in a series of batch kinetic tests (data not shown). The kinetic tests were performed using a pure strain of *Rhodococcus rhodochrous* which was the predominant microbial species found in the VPB biofilm (*21*). To obtain a set of model parameters that optimized the objective function, model simulations were iteratively conducted with combinations of modified parameters within a ±100% range from these starting points. Table 2 presents the model parameters which yielded the best fit (i.e., the minimum SSE) to the actual experimental data. As an example of this iterative fitting process, Figure SI-2 in the Supporting Information illustrates the minimum value of SSE obtained by modifying X_{set} and Y_{act}, while the other parameters were held constant.

A sensitivity analysis was performed on the seven estimated parameters and three initial conditions to determine the ones most critical to model predictions. The impact of each estimated parameter was measured as the change in SSE using eq 11 when each parameter was varied from its nominal value by ±60%, while the other model parameters remained unchanged (Figure SI-3 in the Supporting Information). In addition, sensitivity indexes (i.e., one-point perturbation results) were determined as differences of SSEs between model simulations based on nominal parameter values and the results obtained by increasing each value by 10% (Table 2).

The sensitivity analyses indicate that the mass transfer coefficient (k_L) has the greatest impact on model predictions. This analysis suggests that an accurate estimate of the mass transfer coefficient is needed to increase the accuracy of model predictions and applications. The biomass yield coefficient (Y_{act}), biomass decay coefficient (k_d), and maximum biomass density (X_{set}) are also sensitive parameters affecting model predictions. Alonso et al. (*14*) found that similar parameters in their model, the yield coefficient, decay rate coefficient, and biomass density constant had the greatest impact on model predictions. Since their model and the model developed in this study were both constructed to incorporate biomass growth and decay, sensitivity of the predictions to these parameters was anticipated in both. Experimental methodologies are still under development to determine not only the in situ biochemical characteristics of the biofilm in complex VPB systems but also to directly relate VPB model parameters to these biofilm characteristics. Such methodologies have not been fully established for use in existing CA models even for simple biofilm systems (*18*). For instance, the maximum biomass density (X_{set}) is a conceptual value in this CA model, and extensive research would be required to obtain a more reliable value for model applications.

Model Simulation and Validation. Figure 2 illustrates overall toluene removal efficiencies, toluene concentration profiles, and biomass accumulation along the column for a 90-day simulation of the DS-3-day bioreactor. The simulation results for removal efficiencies and normalized concentration profiles along the column are consistent with experimental findings. In the early phase of bioreactor operation, exponential removal of toluene was observed in the DS-3-day bioreactor. This exponential removal phase was followed by a slow decline in biodegradation activity, resulting in a shift to a near-linear toluene removal profile and eventually toluene breakthrough (less than 95% overall removal efficiency) on day 78 (Figure 2(a)). The model simulation also clearly demonstrates the gradual decline in removal efficiency and the shift in toluene removal from an exponential to a near-linear profile over the 90-day period. The model was used to simulate an additional 22 days after actual bioreactor operation was terminated. On day 90 in the simulation, a removal efficiency of approximately 80% is predicted (Figure 2(a)).

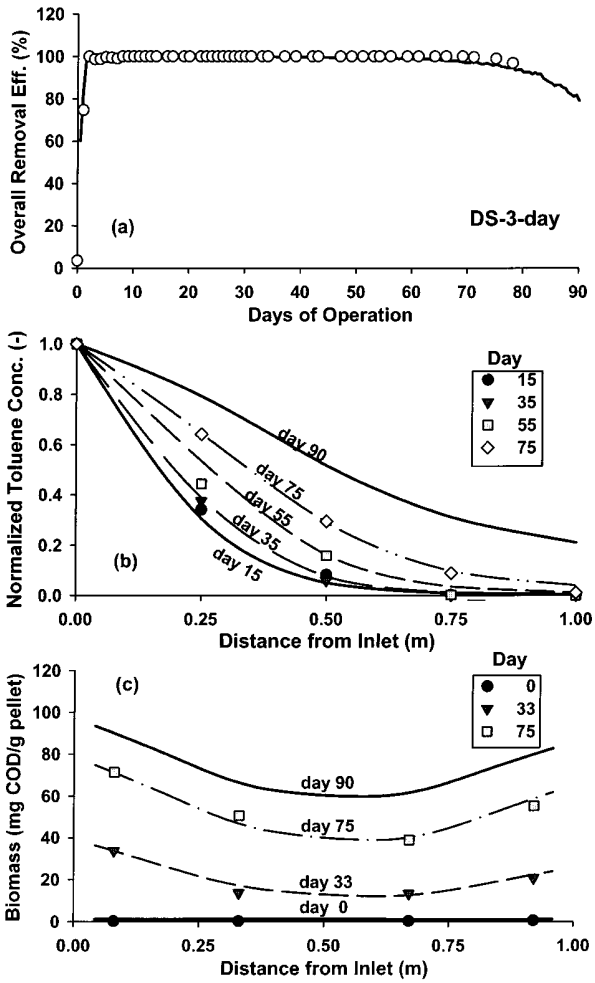

FIGURE 2. Simulation results (lines) and experimental data (symbols) obtained in the DS-3-day bioreactor: (a) overall toluene removal efficiencies, (b) normalized toluene profile along the column, and (c) biomass accumulation.

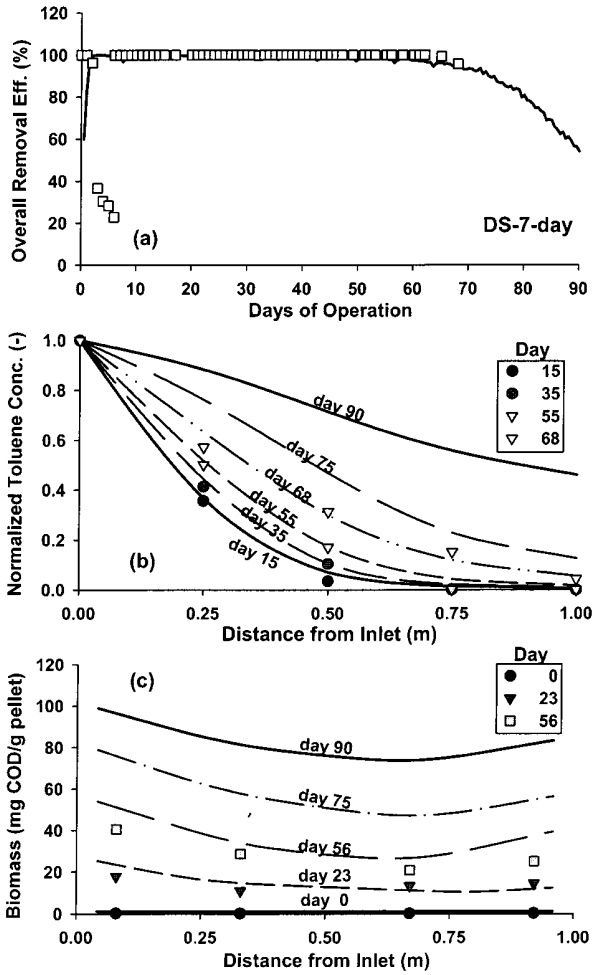

FIGURE 3. Predicted results (lines) and experimental data (symbols) obtained in the DS-7-day bioreactor: (a) overall toluene removal efficiencies, (b) normalized toluene profile along the column, and (c) biomass accumulation.

Figure 2(c) demonstrates that predicted results for the biomass accumulation are consistent with experimental data as a function of operation time. As shown in the figure, biomass accumulated continuously and relatively evenly along the DS-3-day column. Over the 90-day model simulation, biofilm thickness increases by a factor of 24 in the middle of the column and by a factor of 33 near the inlet of the column. As the biofilm thickens, the specific surface area available for mass transfer diminishes correspondingly, and by day 90, the model predicts that the specific surface area in the inlet zone is reduced by 59%. Even though the mass transfer coefficient remains constant, the reduced surface area actually decreases the toluene mass flux into the biofilm. This model prediction suggests that the decrease in specific surface area for mass transfer is one of the key reasons for deterioration in bioreactor performance over extended periods of operation.

Model simulation results for the DS-7-day bioreactor were compared with the experimental data (Figure 3) to validate this model and to test the estimated model parameters determined in the model fitting above. In this experiment, the decline in bioreactor performance in the DS-7-day bioreactor progressed faster than that observed at the DS-3-day, and toluene breakthrough occurred on day 68, i.e., 10 days earlier than that in the DS-3-day bioreactor. The more rapid deterioration in the DS-7-day bioreactor was primarily due to the longer reacclimation period required after each airflow reversal as well as a decline in the toluene-degrading activity in the inlet zone of the column (*21*). The model accurately predicts the decline in performance and toluene breakthrough for the DS-7-day bioreactor over a 90-day simulation. Figure 3(b) demonstrates that the toluene profiles shift more quickly from an exponential to a linear shape with increasing operation time. In addition, as shown in Figure 3(c), a continuous increase in biomass quantity was observed along the DS-7-day column, which is consistent with predicted results.

Model prediction results indicate that the active biomass fraction ($f_{act} = X_{act}/X_{total}$) in the outlet zone of the DS-7-day bioreactor substantially decreases over one cycle of DS operation. For example, the active biomass fraction in the outlet, carbon (toluene) deprived zone of the DS-7-day bioreactor decreases from 81% to 16% over the simulation period between days 7−14. Following each flow direction reversal in DS operation, the new inlet zone of the DS-7-day column requires 72 h to recover biodegradation activity, because it was previously the outlet, carbon deprived zone. This predicted result is consistent with the recovery periods experimentally observed in the DS-7-day bioreactor (*21*). In the DS-3-day bioreactor, model predictions and experimental observations support a less substantial decline in active biomass fraction in the outlet zone.

Overall, this model yields a relatively accurate prediction of VPB performance at different switching frequencies using

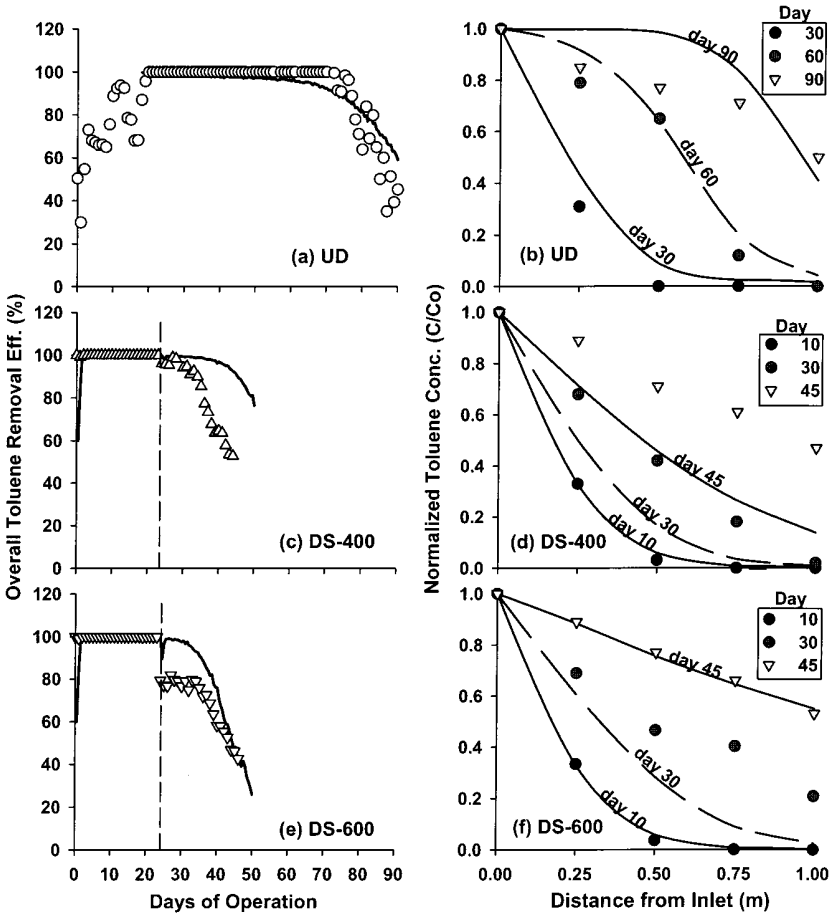

FIGURE 4. Overall toluene removal efficiencies (a, c, and e) and normalized toluene removal profiles along bioreactor columns (b, d, and f) for the UD (unidirectional), the DS-400 and the DS-600 experiments, respectively. Predicted results are indicated as lines and symbols represent measured data. The dotted vertical lines in (c) and (e) indicate the days when loading rates were increased in the DS-400 and DS-600 bioreactors.

the same estimated parameters. In addition, the model simulation provides insight into how biomass accumulation affects the specific surface area and mass transfer of toluene into the biofilm as well as how changes in active biomass have a significant effect on overall biofilter performance. These results suggest that the CA model presented herein is a useful tool for predicting bioreactor performance for extended periods.

Model Application. Model predictions were also compared to experimental results of the unidirectional (UD) bioreactor operation (Figure 4(a) and (b)). During the initial 18-day period, the chemical composition of the nutrient solution supplied to the experimental bioreactor was altered three times to investigate nitrogen requirements and bioreactor start-up performance (*12*). Following this initial period, overall toluene removal efficiencies of greater than 99% were observed. However, bioreactor performance gradually declined over time with increasing biomass accumulation in the inlet zone and pressure drop across the column. The decline eventually resulted in system failure with a rapid drop in overall toluene removal efficiency.

The model simulation of the UD bioreactor was started on day 18 (after the nitrogen limitations had been resolved) with a modified initial biofilm thickness (L_{f0}), while the other parameters remained constant as listed in Table 2. A modified initial biomass thickness of 37.5 μm was selected based on the average biofilm thickness predicted for the DS-3-day column on day 18. As indicated by the ΔSSE value in Table 2, this modification has less impact on model simulations than do the more sensitive parameters such as the mass transfer coefficient and the biomass decay rate. Figure 4(a) illustrates predicted toluene removal efficiencies on days 18–90. Overall, the model predictions agree reasonably with the experimental data, and this model predicts the rapid system failure observed. In addition, predicted toluene removal profiles along the column on days 30 and 60 are consistent with the experimental data (Figure 4(b)). However, in the UD experiment, the removal efficiencies remained greater than 99% until day 70 and then dropped rapidly with increasing pressure drop across the column. In contrast, the model predicts a relatively smooth decline in removal efficiency. The rapid system failure observed in the UD operation was primarily associated with near-complete clogging of the inlet zone and channeling of the airflow. However, the model assumes that biomass accumulates evenly across a given cross-sectional area, and the effect of pressure drop is not incorporated. A potential solution for this extreme clogging condition is to include a pore network algorithm into the model (*26*). In the pore network algorithm, as biomass grows, the open diameter of the pore narrows down, resulting in an increase in pressure drop along the column.

In addition to comparing model predictions to the experimental data from the UD bioreactor, model simulations were conducted for two additional sets of operating conditions at higher toluene inlet concentrations. The two bioreactors (referred to as DS-400 and DS-600 in Table 1) were operated for a period of 45 and 47 days, respectively, to

investigate the effects of high inlet toluene concentrations on bioreactor performance. Both bioreactors were initially operated for 24 days at an inlet toluene concentration of 200 ppm_v identical to that of the DS-3-day bioreactor. On day 24, the inlet concentrations were increased to 400 ppm_v in the DS-400 and 600 ppm_v in the DS-600 bioreactor. After a short pseudo-steady state following the loading increase, a rapid decline in overall removal efficiency was observed in each bioreactor.

Model simulations for these increased concentration conditions were conducted using the same estimated parameters presented in Table 2. Figure 4(c),(e) illustrates toluene removal efficiencies over 50 days of simulation in both bioreactors, and Figure 4(d),(f) shows toluene removal profiles along each column over the operational period. During the initial start-up period, model predictions are consistent with the experimental data. Following the increase in toluene concentration, rapid declines in removal efficiency are predicted in the model simulations for both bioreactors. The model predicts that the biofilm thickness increases much faster at the higher inlet toluene concentrations than at the lower toluene concentrations provided to the DS-3-day bioreactor (e.g., approximately 4.6 times faster overall for the DS-600 than in the DS-3-day). This biomass accumulation results in a rapid decrease in specific surface area and eventually overall removal efficiency. Another interesting finding in the model simulations is that the toluene removal profiles along the column length rapidly shift from exponential curves to linear profiles as VPB performance deteriorates and toluene breakthrough occurs. The toluene removal profile determined experimentally on day 45 of the DS-600 (Figure 4 (f)) is a straight line (R^2 = 99.7%) which agrees well with model predictions.

Despite its reasonable prediction of rapid system failure at high toluene concentrations, this model overestimates bioreactor activity, resulting in a slower decline in predicted removal efficiency than that observed in the DS-400 (Figure 4(c)). The model also predicts higher removal efficiencies immediately after the concentration increase in the DS-600, although the decline is accurately predicted at the end of the simulation (Figure 4(c)). These inaccuracies at higher toluene concentrations may be due to the fact that the model does not consider intrinsic changes that may occur in the kinetic coefficients in the biofilm phase. In a multispecies model developed by Mirpuri et al. (*5*) to predict VPB performance at two different inlet toluene concentrations (150 and 770 ppm_v), the microbial loss coefficients had to be varied to fit the experimental data. In the model simulations presented herein, the biomass decay rate may need to be modified when used to predict the performance of bioreactors subjected to higher toluene concentrations. Nitrogen availability in the biofilm phase may also affect the microbial kinetics (μ_m, K_s, Y_{act}) of the toluene-degrading population. Although the nitrogen supply to both experimental bioreactors was increased following the toluene loading increases to maintain a constant carbon-to-nitrogen ratio, the altered nitrogen supply presumably resulted in a change in microbial kinetics, an effect that is not included in the current formulation of the model. Further investigation of the microbial kinetic parameters would be required to provide better insight into the influence of higher substrate concentrations and nitrogen availability on each individual parameter.

Active Layers and Conventional Models. Changes in concentration profiles of both toluene and active biomass inside the biofilm are predicted using the model. Figure 5(a),(b) illustrate predicted profiles of the active biomass fraction ($f_{act} = X_{act}/X_{total}$) and toluene inside the biofilm near the inlet zone (0.042 m) of the column. On day 15, the active biomass is evenly distributed throughout the biofilm, but

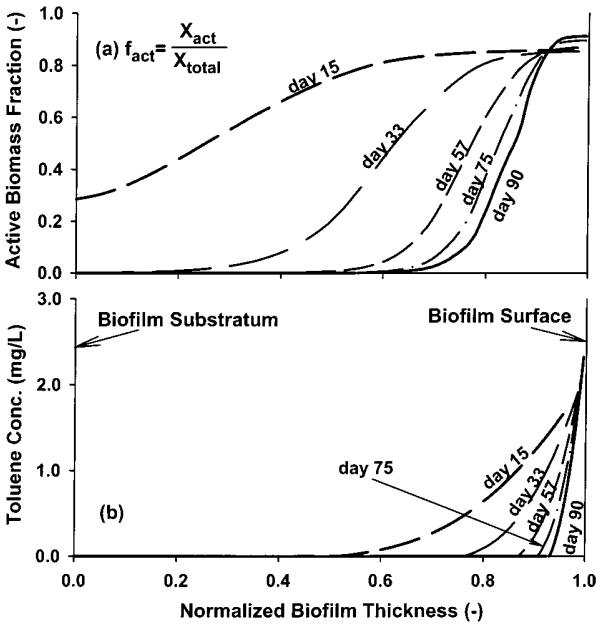

FIGURE 5. Predicted profiles of (a) active biomass fraction (f_{act}) and (b) toluene concentration along the normalized biofilm thickness in the DS-3-day bioreactor, 0.042 m from the contaminated gas inlet. The *x*-axis presents the dimensionless biofilm thickness; thus, a dimensionless thickness of one represents the surface of the biofilm.

the substrate (i.e., toluene) diffuses through only half of the biofilm thickness. As the biofilm thickens, the active biomass shifts toward the biofilm surface, and by day 90, only 40% of the biofilm depth from the surface contains active microbial components. The remaining portion of the biofilm is comprised of inactive biomass only. In this model prediction, the active biomass fraction decreases rapidly from the surface to the substratum of the biofilm (i.e., from 85% to 0%), since toluene degradation takes place in the outermost biofilm. These results suggest that biomass near the bottom of the biofilm suffers from a lack of diffused toluene, resulting in a gradual drop in the quantity of active biomass by endogenous decay. Several studies of simplified biofilm systems have determined the distribution of active biomass and substrate inside biofilms using microelectrodes and microslicing techniques (*27, 28*). These studies have found that substrate and active biomass profiles in thick mixed-culture biofilm are similar to those predicted in this study.

The existence of an active layer (or penetration depth) in a thick biofilm is also assumed in most pseudo-steady-state models developed using simplified assumptions such as zero-order kinetics or first-order kinetics (*1, 2*). These conventional, pseudo-steady-state models generally yield fixed biodegradation rates expressed as exponential functions or square root relationships as a function of column height. These models fail to explain changes in VPB performance and linear removal profiles that develop with time along the column. Only in the case where diffused toluene reaches the bottom of the biofilm (i.e., the reaction-limited condition) do conventional models with zero-order kinetics predict linear removal profiles along the column. However, the reaction-limited condition is not realistic for VPB systems with thick or active biofilms, and many conventional models have relied instead on a diffusion-limited condition based on an active layer concept.

Simplified pseudo-steady-state models are only applicable to limited time periods and operating conditions where model parameters are assumed to remain constant. However, to use these models to predict long-term VPB performance, model parameters must be modified with time, since

significant changes in biomass quantity and activity commonly occur in these systems. The model developed in this study is an important step toward simulating performance under a broader range of bioreactor operating conditions without arbitrary modification of model parameters and should improve our capability to predict long-term performance of VPBs and system failure. This knowledge, in turn, may allow one to develop better biomass control strategies and to determine when a supplementary control method such as backwashing must be applied to maintain stable bioreactor performance.

Nomenclature

a_o and a_f	specific biofilm surface area for clean bed and bed with biofilm (m^2/m^3)
C_g and C_l	toluene concentrations in the gas and biofilm phases (mg/L_{gas})
$C_{l,x=Lf}$	toluene concentration at the biofilm interface (mg/L_{liquid})
D_f	effective diffusion coefficient of toluene in the biofilm phase (m^2/h)
$f_{measured}$	experimentally measured value used for parameter estimation
f(p)	simulated values using a set of estimated parameters
H	Henry's law constant for toluene (mg/L_{gas}/ mg/L_{liquid})
J	diffusive flux of toluene from the gas phase to the biofilm (mg/m^2-h)
K_s	Monod half saturation constant (mg/L)
k_d	biomass decay rate (1/h)
k_L	mass transfer coefficient (m/h)
L_f and L_i	biofilm thickness and interface thickness (m)
N	number of biofilm elements in a layer
n	coordinate number of the characteristic packing spheres in contact with a given sphere (−)
p	set of estimated parameters
R	characteristic packing sphere radius (m)
v	superficial gas velocity (m/h)
W	dimension (width) of each biofilm element (m)
w_i	weighting factor for the parameter estimation
X_{act} and X_{inact}	biomass densities of the active and inactive microbial components (mg COD/L)
$X^i_{act}(t)$ and $X^i_{inact}(t)$	biomass densities of the active and inactive microbial components in the *i*th biofilm element at time *t* (mg/L)
X^i_{total}	sum of the active and inactive microbial components in the *i*th biofilm element (mg/L)
X_{set}	maximum biomass density allowable in a biofilm grid element (mg/L)
X_{excess}	excess biomass quantity grater than X_{set} in a biofilm grid element (mg/L)
$X^i_{act}(t^*)$ and $X^i_{inact}(t^*)$	biomass densities of the active and inactive microbial components in the *i*th biofilm after the excess biomass quantity has been transferred from the element (mg/L)
Y_{act}	yield coefficient of X_{act} (mg $COD_{biomass}$/ $mg_{toluene}$)

Greek Letters

β	formation coefficient of X_{inert} (−)
ϵ_o and ϵ_f	clean bed porosity and bed porosity of the packed column (m^3 void space/m^3 reactor volume)
ϕ	sphericity factor of pelletized packing materials (−)
μ_m	maximum growth rate of X_{act} (1/h)

Acknowledgments

This research was funded by the U.S. Environmental Protection Agency (Grant No. R826168-01-0) and the Strategic Environmental Research and Development Program (Grant No. F08637-98-C-6005). The results and conclusions expressed in this publication are solely those of the authors and do not necessarily reflect the view of the sponsors. The authors would also like to thank the anonymous reviewers for their helpful comments.

Supporting Information Available

Figures showing (1) schematic of the experimental bioreactor system, (2) an example of the model parameter estimation process, and (3) results of the sensitivity analysis for the estimated model parameters. These materials are available free of charge via the Internet at http://pubs.acs.org.

Literature Cited

(1) Ottengraf, S. P. P.; van den Oever, A. H. C. *Biotechnol. Bioeng.* **1983**, 25, 3089−3102.
(2) Ottengraf, S. P. P. In *Biotechnology*, v.8; Rehm, H. J., Reed, G., VCH Verlagsgesellschaft: Weinheim, Germany, 1986; pp 425−452.
(3) Pedersen, A. R.; Arvin, E. *Biodegradation* **1995**, *6*, 109−118.
(4) Shareefdeen, Z.; Baltzis, B. C. *Chem. Eng. Sci.* **1994**, *49*, 4347−4360.
(5) Mirpuri, R.; Sharp, W.; Villaverde, S.; Jones, W.; Lewandowski, Z.; Cunningham, A. *J. Environ. Eng.* **1997**, *123*, 586−592.
(6) Deshusses, M. A.; Hamer, G.; Dunn, I. J. *Environ. Sci. Technol.* **1995**, *29*, 1048−1058.
(7) Cherry, R. S.; Thompson, D. N. *Biotech., Bioeng.* **1997**, *56*, 330−339.
(8) Hodge, D. S.; Devinny, J. S. *J. Environ. Eng.* **1995**, *121*, 21−32.
(9) Okkerse, W. J. H.; Ottengraf, S. P. P.; Osinga-Kuipers, B.; Okkerse, M. *Biotech., Bioeng.* **1999**, *63*, 418−430.
(10) Kinney, K. A.; Loehr, R. C.; Corsi, R. L. *Environ. Prog.* **1999**, *18*, 222−230.
(11) Mirpuri, R.; Jones, W.; Bryers, J. D. *Biotechnol. Bioeng.* **1997**, *53*, 535−546.
(12) Song, J.; Kinney, K. A. *Biotechnol. Bioeng.* **2000**, *68*, 508−516.
(13) Smith, F. L.; Sorial, G. A.; Suidan, M. T.; Breen, A. W.; Biswas, P. *Environ. Sci. Technol.* **1996**, *30*, 1744−1751.
(14) Alonso, C.; Suidan, M. T.; Sorial, G. A.; Smith, F. L.; Biswas, P.; Smith, P. J.; Brenner, R. C. *Biotechnol. Bioeng.* **1997**, *54*, 583−594.
(15) Alonso, C.; Suidan, M. T.; Kim, B. R.; Kim, B. J. *Environ. Sci. Technol.* **1998**, *32*, 3118−3123.
(16) Wanner, O. *Water Sci. Technol.* **1995**, *32*, 133−140.
(17) Noguera, D. R.; Pizarro, G.; Stahl, D. A.; Rittmann, B. E. *Water Sci. Technol.* **1999**, *39*(7), 123−130.
(18) Pizarro, G.; Griffeath, D.; Noguera, D. R. *J. Environ. Eng.* **2001**, *127*, 782−789.

(19) Picioreanu, C.; van Loosdrecht, M. C. M.; Heijnen, J. J. *Biotechnol. Bioeng.* **1998**, *58*, 101−116.
(20) Picioreanu, C.; van Loosdrecht, M. C. M.; Heijnen, J. J. *Biotechnol. Bioeng.* **2000**, *68*, 355−369.
(21) Song, J.; Kinney, K. A. *Appl. Microbiol. Biotechnol.* **2001**, *56*, 108−113.
(22) Gerald, C. F.; Wheatley, P. O. *Applied Numerical Analysis*, 5th ed.; Addison-Wesley Publishing Co.: New York, 1994; p 230.
(23) Alonso, C.; Zhu, X.; Suidan, M. T.; Kim, B. R.; Kim, B. J. *Environ. Sci. Technol.* **2000**, *34*, 2318−2323.
(24) Pedersen, A. R.; Arvin, E. *Water Sci. Technol.* **1999**, *39*, 131−137.
(25) Shareefdeen, Z.; Baltzis, B. C. *Chem. Eng. Sci.* **1994**, *49*, 4347−4360.
(26) Schwarz, B. C. E.; Nukunya, T.; Devinny, J. S.; Tsotsis, T. T. In *Proceedings of 2000 USC-TRG Conference on Biofiltration*; LA, CA, October 19−23, 2000; pp 167−174.
(27) Zhang, T. C.; Fu, Y.-C.; Bishop, P. L. *Water Environ. Res.* **1995**, *67*, 992−1003.
(28) Okabe, S.; Hiratia, K.; Ozawa, Y.; Watanabe, Y. *Biotechnol. Bioeng.* **1996**, *50*, 24−35.

Received for review July 20, 2001. Revised manuscript received March 27, 2002. Accepted April 5, 2002.

ES0156183